LAWRENCE
LIVERMORE
NATIONAL
LABORATORY

UCRL-TR-205282

Calculating Sensitivities, Response and Uncertainties Within LODI for Precipitation Scavenging

Gwen Loosmore, Henry Hsieh, Keith Grant

July 16, 2004

This work was performed under the auspices of the U.S. Department of Energy by University of California, Lawrence Livermore National Laboratory under Contract W-7405-Eng-48.

Calculating wet deposition sensitivities and uncertainties within a Lagrangian particle dispersion code

Gwen Loosmore
Henry Hsieh
Keith Grant
6/11/2004

Introduction

This paper describes an investigation into the uses of first-order, local sensitivity analysis in a Lagrangian dispersion code. The goal of the project is to gain knowledge not only about the sensitivity of the dispersion code predictions to the specific input parameters of interest, but also to better understand the uses and limitations of sensitivity analysis within such a context. The dispersion code of interest here is LODI [1], which is used for modeling emergency release scenarios at the Department of Energy's National Atmospheric Release Advisory Center (NARAC) at Lawrence Livermore National Laboratory. The NARAC system provides both real-time operational predictions and detailed assessments for atmospheric releases of hazardous materials. LODI is driven by a meteorological data assimilation model [2] and an in-house version of COAMPS [3], the Naval Research Laboratory's mesoscale weather forecast model.

There is increasing interest in the development of uncertainty quantification tools for NARAC and other computational models at LLNL. Monte Carlo and ensemble techniques are available but computationally expensive. Sensitivity analysis is being explored as a means to gain an understanding of the contribution to uncertainty from certain types of input parameters. As a first step, first-order sensitivity analysis was implemented within the precipitation-scavenging module of LODI. This module is logically split from the remainder of the dispersion calculation, so the sensitivities may be explored without concern about parameter and computational dependencies, and the linearization implicit in the formulation is acceptable. The general goals of the project are:

1. To understand the sensitivity of LODI predictions of precipitation scavenging (wet deposition) to the rain rate and aerosol particle size
2. To explore the advantages and limitations of first-order sensitivity analysis within a Lagrangian dispersion framework
3. To gain the understanding necessary to plan a more comprehensive uncertainty analysis project for the NARAC suite of codes

The following text describes the mathematical foundation of the sensitivity analysis and its implementation within LODI. Later sections present specific results.

Mathematical Background

First-order sensitivity analysis consists of a mathematical exploration of the response of a computed output to a perturbation in the input parameters. For example, given a differential equation for an n-dimensional vector *y*, expressed:

$$\dot{y} = f(t, y, p) \qquad \textbf{eq. 1}$$

where *p* is an m-dimensional vector of parameters $[p_1, p_2, \ldots, p_m]^T$, we assume that a perturbation δp_j causes a response in y_i of magnitude δy_i, relative to the nominal value $y_{i,o}$, where the relationships are assumed to be linear:

$$\delta y_i = y_i - y_{i,o} = \frac{\partial y_i}{\partial p_j}\delta p_j = S_{ij}\delta p_j \qquad \textbf{eq. 2}$$

The sensitivity matrix *S* is defined as the first-order relationship between the dependent variable *y* and the parameters *p*:

$$S_{ij} = \frac{\partial y_i}{\partial p_j} \qquad \textbf{eq. 3}$$

The total response of y_i to the perturbation vector (for discrete perturbations) may be obtained through a Taylor expansion as:

$$\delta y_i = \sum_j S_{ij}\delta p_j \qquad \textbf{eq. 4}$$

Generally, we can write:

$$(\delta y)(\delta y)^T = \frac{\partial y}{\partial p}\delta p \delta p^T \left(\frac{\partial y}{\partial p}\right)^T = S\delta p \delta p^T S^T \qquad \textbf{eq. 5}$$

The parameter perturbations may be generated from k statistical samples around the nominal value, in which case the middle term $\delta p \delta p^T$ should be divided by k to produce an average, yielding an m×m matrix. Equation 6 describes the relationship between the covariance matrix for *y*, C_y and the covariance matrix for δp, C_p:

$$C_y = SC_pS^T \qquad \textbf{eq. 6}$$

If the statistical perturbations in the parameters are uncorrelated, (i.e. if the parameters are uncorrelated), then C_p will be diagonal. In this case the form will be simplified from the full Taylor series, as the cross terms will be eliminated. An example (for precipitation scavenging) is given later in the paper.

Precipitation Scavenging in LODI

LODI is a Lagrangian particle code in which pseudo particles, representing groups of simulated aerosol particles from a specified size distribution, travel through a computational domain that represents the atmosphere. Each particle contains mass that may be lost through precipitation scavenging, following a first-order decay equation:

$$\dot{M} = -\lambda M \qquad \textbf{eq. 7}$$

The scavenging coefficient λ is a function of the rain rate and aerosol particle diameter. This coefficient includes the effects of both the capture efficiency of a particular raindrop and the volume of air swept by the raindrops, given a rain rate. Streamlines are created around a falling raindrop, and the capture efficiency includes Brownian diffusion, interception, and impaction, a subset of the processes that affect whether the aerosol particle can effectively follow the streamlines past the raindrop and escape. The dependence of λ on these parameters is shown in Figure 1. A more complete explanation of the theoretical underpinnings and computation of λ is found in [4].

Figure 1: Scavenging coefficient λ, as a function of particle size and rain rate

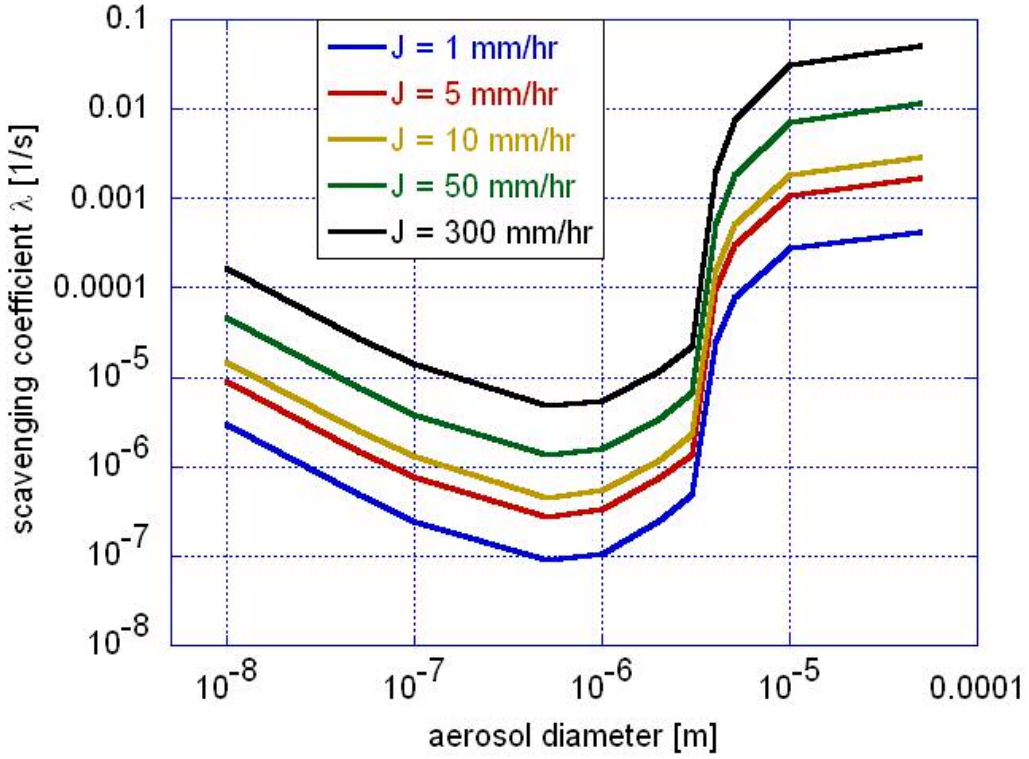

There are several features of the shape of the curves in Figure 1 that indicate important sensitivities. First, λ spans six orders of magnitude for the parameter values shown. For a given particle size, the rain rate can change λ by almost two orders of magnitude; λ varies dramatically across particle sizes. There are three important particle size regimes. In the smallest, for particles up to roughly $5x10^{-7}$ microns, the dominant capture mechanism is Brownian diffusion; the smaller particles with higher diffusivities are captured most efficiently. At the other end of the spectrum, the largest aerosol particles cannot follow the fluid streamlines and instead impact the raindrop directly; whether this can happen depends on a critical Stokes number for collection, creating a discontinuity in the scavenging coefficient at a particle size of ~3.3 microns (for unit density particles) as seen in Figure 2. The middle range of particle sizes have small diffusivities and will not directly impact, hence they are poorly captured.

Figure 2: The discontinuity in the calculation of λ, resulting from Stokes number considerations

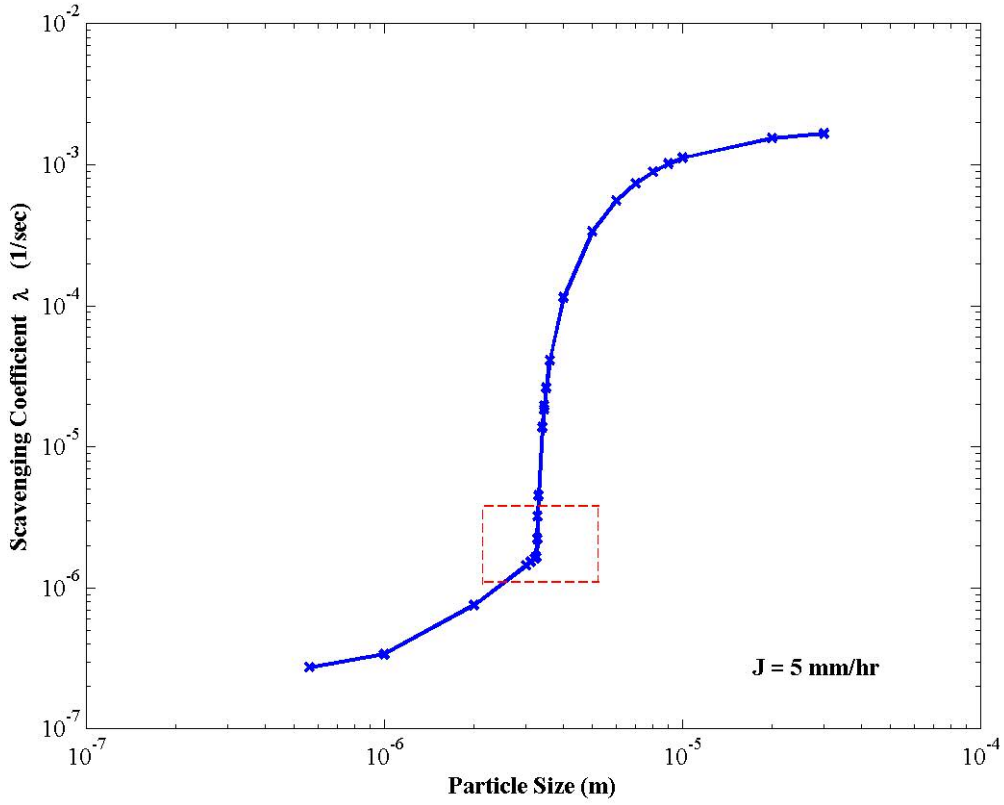

An example calculation of the decay process (i.e. equation 7) is presented in Figure 3. Here the particle diameter is fixed at 5 microns, and the rain rate varies from 1 to 150 mm/hr. Not unexpectedly, less mass is removed in the early time for the particles with the smallest scavenging coefficients.

Figure 3: Evolving particle mass as a function of the scavenging coefficient

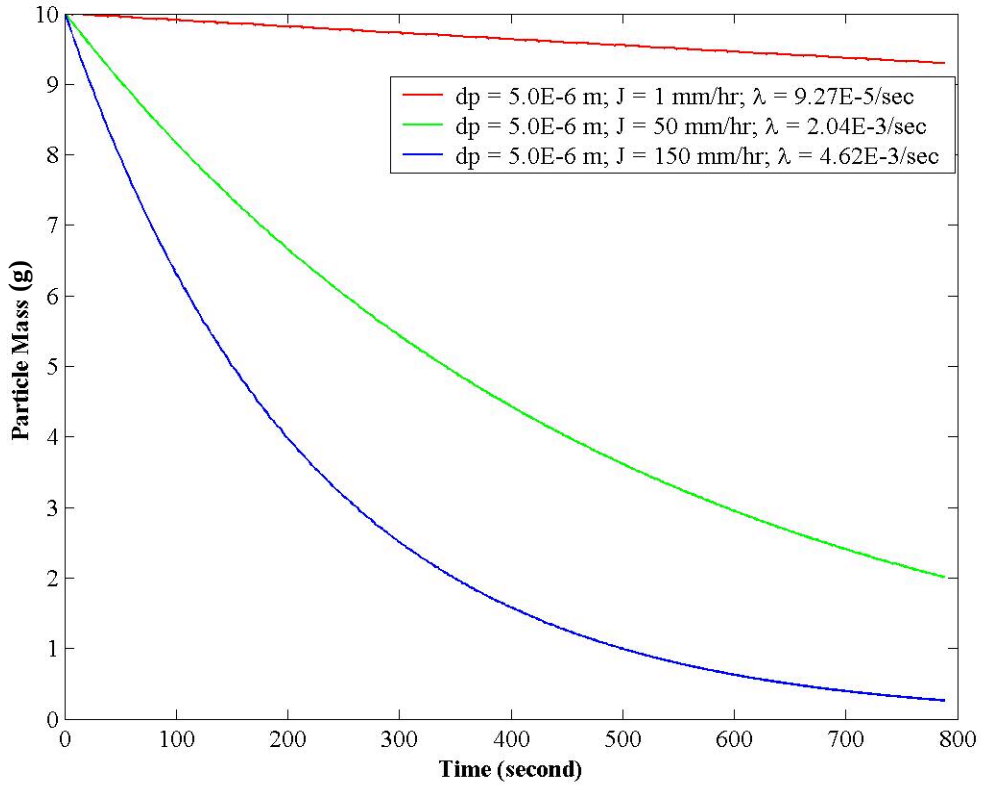

Within LODI, the scavenging coefficient is calculated dynamically, using the particle size and the rain rate interpolated from a 2-D gridded field to the particle's location. The particle mass is depleted as appropriate for the time step, and the scavenged mass is added to a 2-D deposition array representing the appropriate location on the ground. Deposits from different particles are accumulated. At relevant times of interest the spatially varying air concentration is obtained by summing over the mass of particles in a grid cell volume. Our interest is in quantifying the sensitivities of the deposited mass and air concentrations to the rain rate and particle size.

Sensitivity Analysis in the LODI Precipitation Scavenging Module

Because precipitation scavenging depends on the two parameters J (rain rate) and d_p (particle size), two sensitivities are tracked over time for each particle. For expository purposes the paper first explains the computation of sensitivity with respect to d_p; the calculation of the sensitivity with respect to J is analogous. Discussion of the integration and use of the two sensitivities follows. We define the sensitivity *S* of the particle's mass M (for a particle *i* at time *t*), to the particle size d_p as:

$$S_i(t) \equiv d_p \frac{\partial M_i}{\partial d_p}(t) = \frac{\partial M_i}{\partial \ln(d_p)}(t) \qquad \textbf{eq. 8}$$

The normalization by d_p is for convenience in the specification of the uncertainty for d_p. The response of the particle (which may be interpreted as an uncertainty in the mass) to a given *relative* uncertainty in particle size (denoted here by σ_{dp}) is given by:

$$\Delta M_i(t) \equiv \delta d_p \frac{\partial M_i}{\partial d_p}(t) = \frac{\delta d_p}{d_p} \frac{\partial M_i}{\partial \ln(d_p)}(t) = \frac{\delta d_p}{d_p} S_i(t) = \sigma_{dp} S_i(t) \qquad \textbf{eq. 9}$$

Note here that sensitivities are typically negative: higher rain rates promote more mass removal, and the sign indicates this negative correlation.

An equation for the evolution of the sensitivity of a particle *i* at time *t* may be derived from the equation for the evolution of mass in time, (treating $\ln(d_p)$ as time-invariant):

$$\begin{aligned} \dot{S}_i &= \frac{\partial}{\partial t}\left(\frac{\partial M_i}{\partial \ln(d_p)}\right) = \frac{\partial}{\partial \ln(d_p)}\left(\frac{\partial M_i}{\partial t}\right) = \frac{\partial}{\partial \ln(d_p)}\left(-\lambda M_i\right) \\ &= -\lambda \frac{\partial M_i}{\partial \ln(d_p)} - M_i \frac{\partial \lambda}{\partial \ln(d_p)} \qquad \textbf{eq. 10} \\ &= -\lambda S_i - M_i \frac{\partial \lambda}{\partial \ln(d_p)} \end{aligned}$$

For constant in time λ, this equation has an analytic solution, which we use for testing:

$$S_i(t) = S_i(0) e^{-\lambda t} - M_i(0) \frac{\partial \lambda}{\partial \ln(d_p)} t e^{-\lambda t} \qquad \textbf{eq. 11}$$

We assume that the initial sensitivity is zero, for generality. A sample analytic solution is plotted in Figure 4, below. For a fixed rain rate, $\partial\lambda/\partial(\ln(d_p))$ is constant, so the sensitivity follows $te^{-\lambda t}$. The sensitivity peaks in magnitude at $t = 1/\lambda$. For $t > 1/\lambda$, the response of the particle to a perturbation in the rain rate shrinks over time. This trend can be observed in Figure 4, in which the sensitivity to particle size, S_{dp}, is presented. The analytic solution for S_J shows the same behavior.

The equation for the decay of particle mass with rain rate is solved within LODI as:

$$\Delta m_i = M_i(t)\left(1 - e^{-\lambda \Delta t}\right) \qquad \textbf{eq. 12}$$

where Δm is the mass removed from the particle (and added to the deposition array) in the time step Δt.

Given this explicit approach to the solution of the mass equation, we take a similar approach to the solution of the sensitivity equation, discretizing as:

$$S_i(t_{n+1}) = S_i(t_n)(1-\lambda\Delta t) - \Delta t M_i(t_n)\frac{\partial\lambda}{\partial \ln(d_p)}(t_n) \qquad \textbf{eq. 13}$$

If the time step chosen is appropriate for the mass equation, it will also be sufficient for the sensitivity equation. Within LODI the time step is limited by a variety of processes; the limitation for precipitation scavenging is $\Delta t \leq 1/8\lambda$. We obtain satisfactory computational solutions to equation 10 within the limits of this Δt, as shown in Figure 4; the agreement is improved by using a smaller time step, as expected.

Figure 4: Comparison of analytic and computational solutions to sensitivity

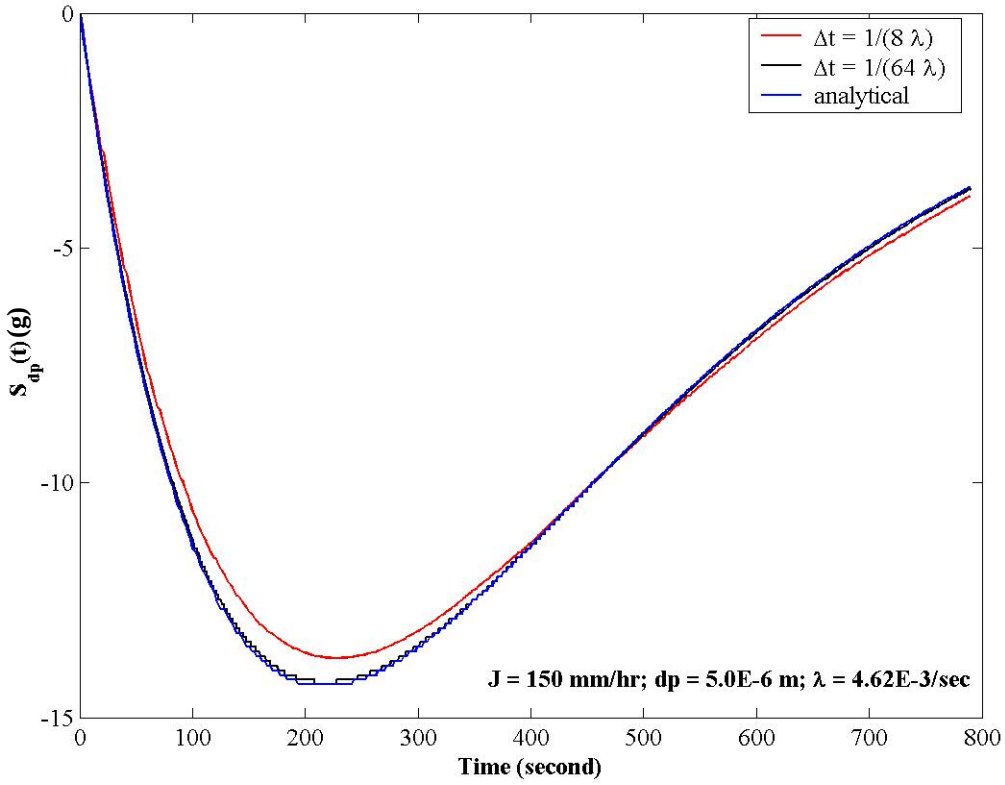

The gradient of λ is computed with a simple forward difference, using a small perturbation ε:

$$\frac{\partial\lambda}{\partial \ln(d_p)} = d_p\frac{\partial\lambda}{\partial d_p} \cong d_p\frac{\lambda(d_p+\varepsilon d_p)-\lambda(d_p)}{\varepsilon d_p} \qquad \textbf{eq. 14}$$

Because of the apparent strong sensitivity of λ to particle size, as seen in Figure 1, and because the equation for sensitivity depends on the gradient of λ with respect to particle

size, we wanted to ensure that the computation of that gradient was correct. Thus we investigated the use of different sizes of perturbation as well as the difference between forward and centered differences. The effects of different perturbations (ε) on the gradient computation are shown in Figure 5.

Figure 5: Effect of perturbation size on gradient estimation (see text for details)

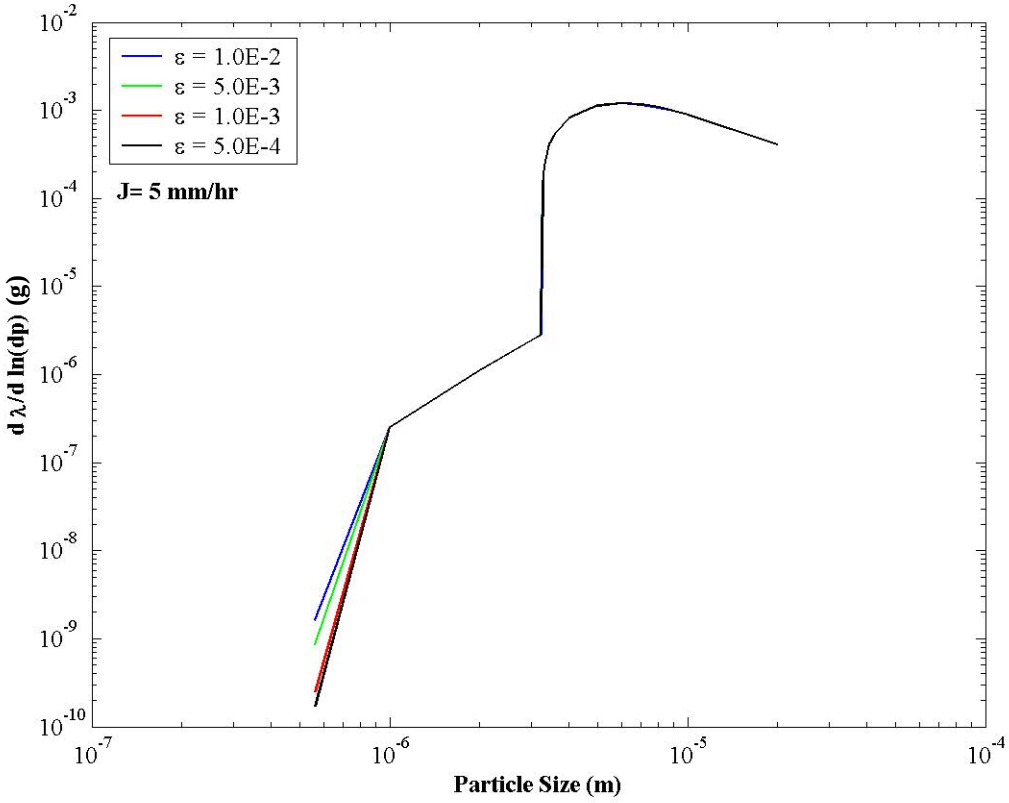

While the larger perturbation would be sufficient for most of the particle sizes of interest, the gradient diverges significantly for particles of size 0.5 to 1 micron. Hence, a uniform value of 1.0e-3 was used for the perturbation value for particles ranging from 0.5 to 4 microns, in the results shown below. The effect of the perturbation on particles smaller than about 5e-7 m is negligible and is not shown, as the gradient is negative in this region.

The difference between the forward and central difference approximations are shown in Figure 6, below. The difference is largest at the impaction discontinuity, and since this was a deviation of only 10%, we use forward differences for all particle sizes.

Figure 6: Use of different approximations for the derivative

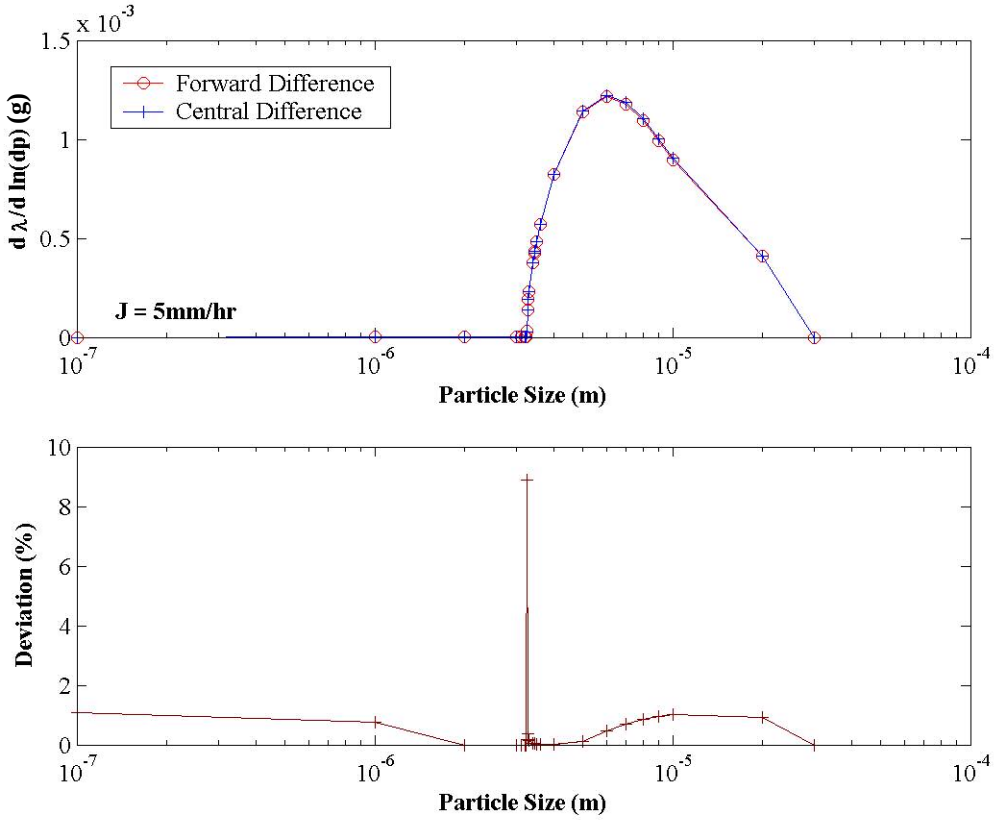

Figure 7 contrasts the sensitivity to particle size and rain rate, for a constant rain rate of 5 mm/hr, for the range of particle sizes of interest. Each data point represents the sensitivity of an individual particle's mass to either its particle size or the rain rate. Computed data points are indicated with symbols and connected by lines. Sensitivity is a function of time: the plot shows just the sensitivities computed at the end of the first time step of the calculation. Later time steps show similar trends, as would be expected from the form of the equation (see figures 23 and 24, below).

Figure 7: Magnitudes of sensitivities to particle size and rain rate (following the first time step)

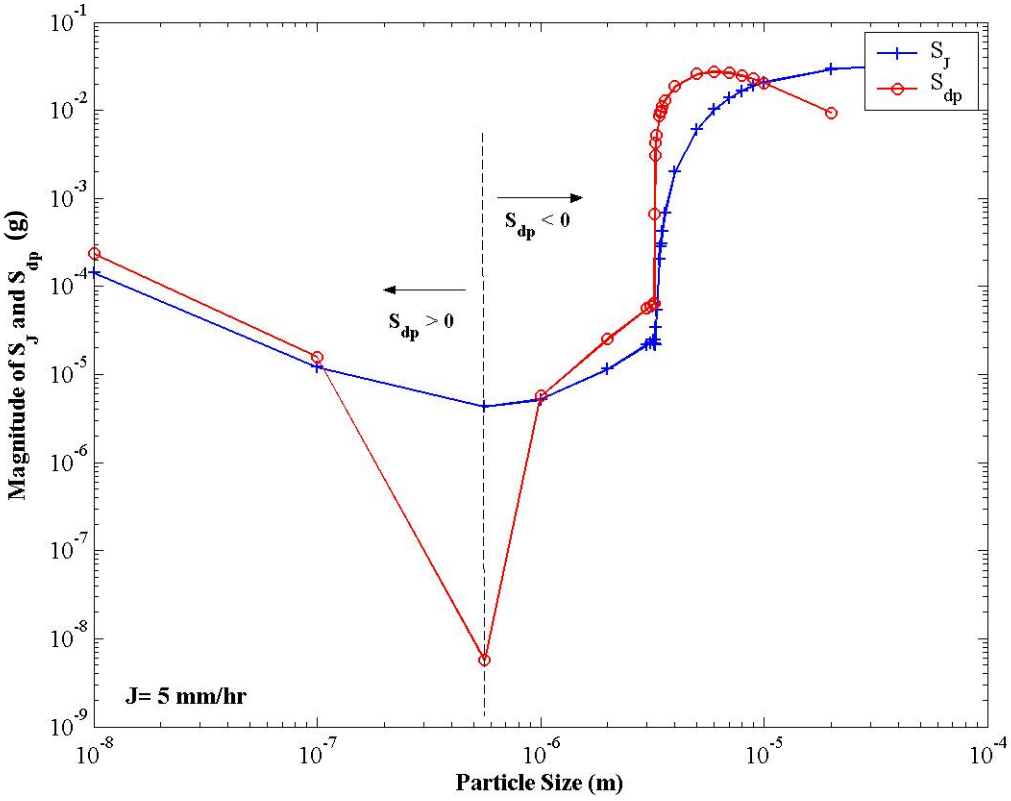

All sensitivities are negative, except S_{dp} for particles smaller than ~5.6e-7 m. These positive sensitivities reflect the trend of the scavenging coefficient with particle size in this regime: increasing particle size results in smaller values for λ. Less mass is scavenged from the particle with a smaller λ, hence S_{dp} (which represents the trend of particle mass with particle size) is positive. All other sensitivities are negative, implying that an increase in the parameter (particle size or rain rate) would cause more mass to be scavenged from the particle.

Four distinct regions can be observed. For the smallest particle sizes considered, 10^{-8} and 10^{-7} m, the magnitude of S_{dp} is slightly greater than S_J. The magnitude of S_{dp} drops below that of S_J at the minimum of the Greenfield Gap, around 0.5 microns, where S_{dp} changes sign. From roughly 0.5 to 10 microns, the magnitude of S_{dp} exceeds that of S_J, and then for larger particles S_J becomes more important again. There is a steep jump in both sensitivities for at a particle aerodynamic diameter of ~3.3 microns, where impaction becomes possible (mimicking the jump in the scavenging coefficient curve).

The sensitivity of the particle mass to wet deposition is zero for large particle sizes: lambda approaches a constant value (as seen in Figure 1), so the gradient becomes zero. In other words, increasing particle size does not affect the scavenging coefficient. Hence no value for S_{dp} has been plotted on this scale for $d_p \geq$ 2e-5 m. Particles smaller than 10

microns pose the greatest danger through inhalation. For much of this regime, the sensitivities to the two parameters have the same magnitude, indicating that both are important. This is a key result of the study. A large improvement in accuracy in only one of the parameters will likely not provide a large improvement in the prediction fidelity.

Expansion of Analysis to Multiple Parameters

In order to compute the overall uncertainty in particle mass, the two sensitivities must be considered together. Here the sensitivity is a 1×2 matrix:

$$S = \left[\frac{\partial M}{\partial(\ln J)} \quad \frac{\partial M}{\partial(\ln d_p)} \right] \qquad \textbf{eq. 15}$$

Because the particle size d_p and the rain rate J are uncorrelated, the covariance matrix is simply:

$$C_p = \begin{pmatrix} \sigma_J^2 & 0 \\ 0 & \sigma_{dp}^2 \end{pmatrix} \qquad \textbf{eq. 16}$$

where the variances represent the relative uncertainty in the parameters. We are interested in perturbations in particle mass M. Making use of equation 5, the uncertainty of the mass is computed from the sum of the squares of the products of the sensitivities and relative uncertainties in J and d_p.

$$(\delta M)^2 = (S_J \sigma_J)^2 + (S_{d_p} \sigma_{dp})^2 \qquad \textbf{eq. 17}$$

Note that equation 4, which predicts a response to a specific perturbation, can be expressed:

$$(\delta M)^2 = \left(S_J \frac{\delta J}{J} \right)^2 + \left(S_{d_p} \frac{\delta d_p}{d_p} \right)^2 + 2 S_J \frac{\delta J}{J} S_{d_p} \frac{\delta d_p}{d_p} \qquad \textbf{eq. 18}$$

When the response of M is computed over many samples of perturbations in J and d_p (or from a statistical representation), the cross term represents the correlation between the perturbations, which will be zero in our case, and the perturbations in the squared terms become the statistical variances of the perturbations, as in equation 17.

To use the sensitivities in the calculation of uncertainty, we need to specify the relative uncertainties for the input parameters. The true relative uncertainty will be dependent on the circumstances. For the following example, we assume that the relative uncertainties

(σ_J and σ_{dp}) in rain rate and particle size are 10 percent, i.e.: $\delta J/J = \delta d_p/d_p = 0.1$. These results are shown in Figure 8.

Figure 8: Uncertainty in particle mass following the first time step

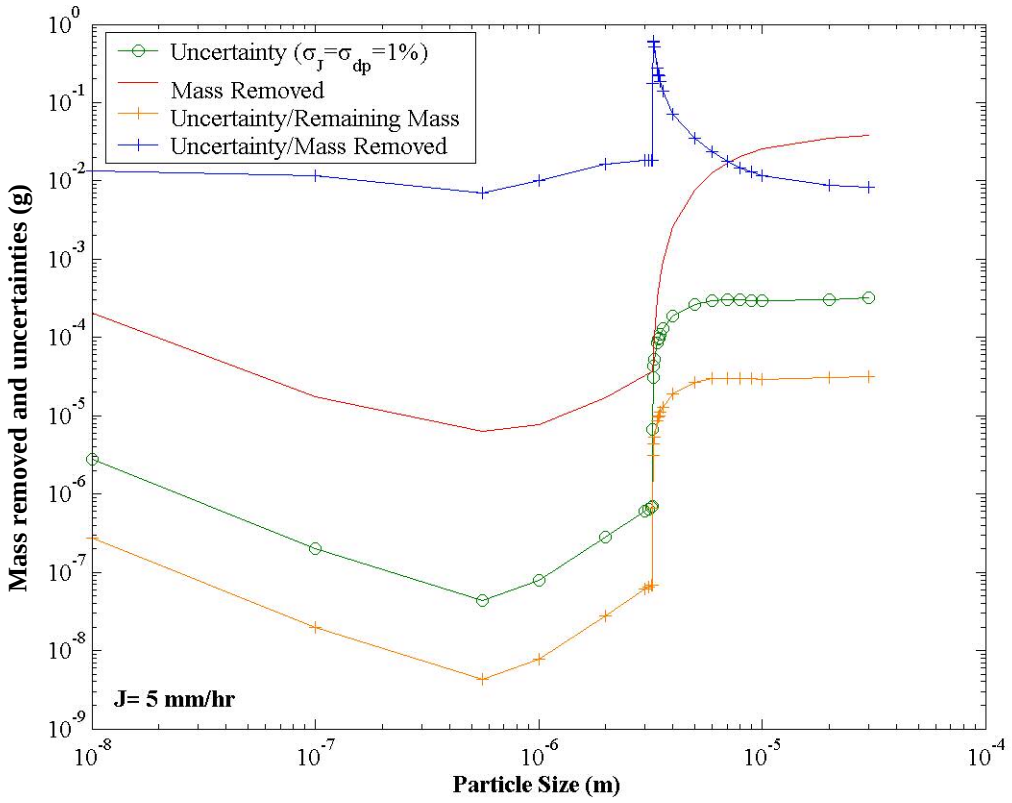

Here the trend follows the sum of the sensitivities plotted in Figure 7. The uncertainty normalized by the mass removed peaks at the discontinuity, where substantially more mass is removed.

A suite of single-particle simulations is presented in the appendix, demonstrating the effects of different relative uncertainties on particle mass uncertainties, for various particle sizes and rain rates.

Air Concentration Uncertainty

The sensitivities and uncertainties in particle mass are used to compute the overall uncertainty in predicted air concentrations as follows. The concentration C, composed of a nominal concentration value C_o and the associated uncertainty δC, is computed by summing particle mass in a given volume:

$$C = C_o + \delta C$$
$$= \frac{M_o + \sqrt{(\delta M)^2}}{V} \qquad \textbf{eq. 19}$$
$$= \frac{\sum_i \left(M_i + \sqrt{\sum_j \left(s_{i,j}\sigma_j \right)^2} \right)}{V}$$

where i represents the sum over all particles in the volume V, and j represents the sum over the perturbed parameters of interest. Thus the uncertainty in air concentration may be computed simultaneously with the air concentration itself, using the sensitivities associated with the particles in the volume of interest.

Air concentration uncertainties resulting from wet deposition were computed for a simulated 15-hour rainfall event. The test simulation used precipitation data from an inhomogeneous event crossing through north-central Oklahoma and south-central Kansas on July 18, 1997. Observed meteorological data from the DOE Atmospheric Radiation Measurement Program provided the near-surface winds every 30 minutes and vertical profiles of winds every 3 hours. The 4-km, hourly precipitation data set was computed at the Arkansas Red-Basin River Forecast Center, using reflectivity from numerous weather radars and observed precipitation from over 100 rain gauges. The simulation was executed on a 4 km grid; rain rates were interpolated from the grid to the Lagrangian particle locations at each time step. The simulated contaminant aerosol source emitted continuously in the southeast corner of the domain, at 10 m height, at a location expected to be buffeted by the storm. A total of 200,000 particles were used for the 15-hour release. A post-processor smoothing algorithm (1:2:1 filter) was used to smooth anomalies introduced by discrete particles. The uncertainty of the air concentration was computed assuming relative uncertainties of 1%. This number was chosen arbitrarily for illustration.

The air concentration plume after 8 hours of simulation is shown in Figure 9 below. The contours represent concentration levels separated by factors of 10 (i.e., 0.1-1 units/volume, 1-10 units/volume, etc.). The uncertainty associated with this air concentration plume is also shown. The uncertainty plot is contoured at levels 1/1000 that of the air concentration plot. Two important features emerge: (1) the uncertainty is not uniform over the domain, and (2) there are high concentrations of uncertainty in areas most affected by the plume, as would be expected.

Figure 9: Air concentration (at left) and associated uncertainty (contoured at 1/1000 of air concentration) (at right)

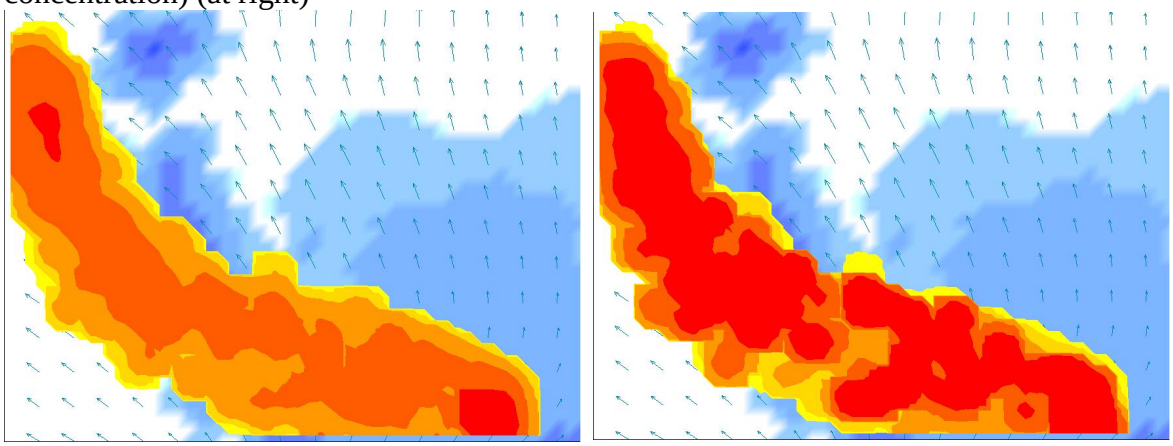

It is desirable to use the uncertainties to establish “error bars” on the prediction, perhaps by showing contours of the air concentration plume ± the uncertainty, as in Figure 10. However, for this example the uncertainty is small relative to the air concentration for this problem, and such contours are virtually indistinguishable.

Figure 10: Air concentration ± uncertainty

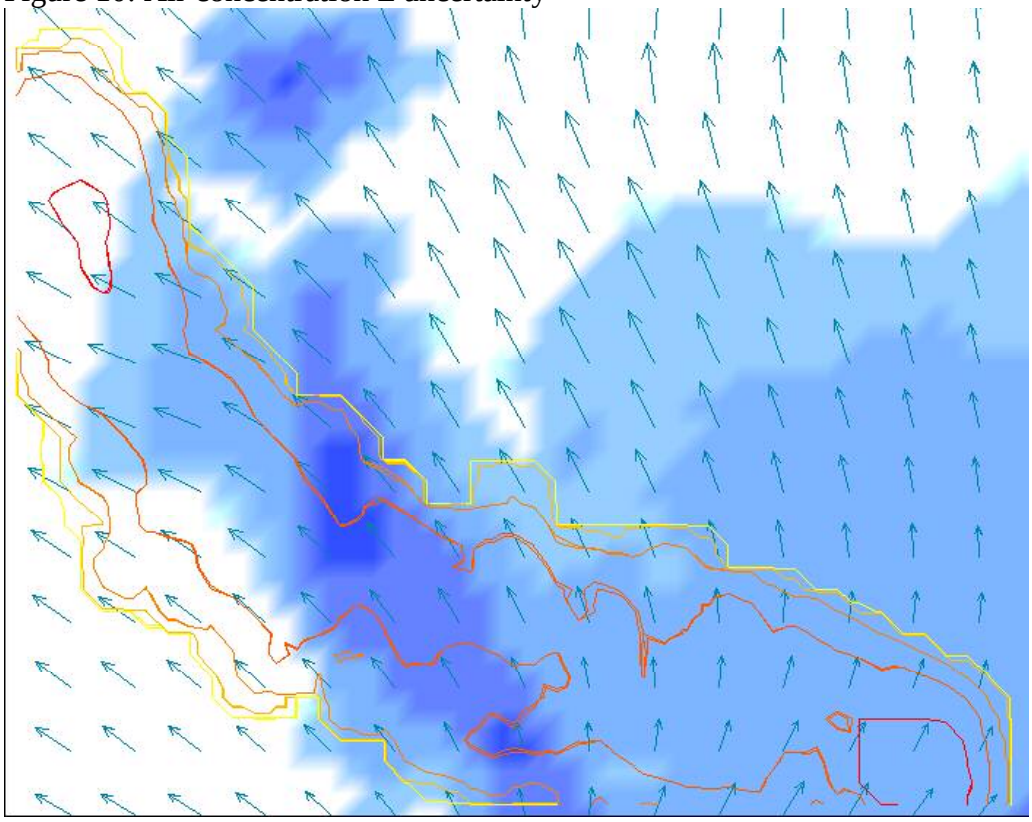

Uncertainty of Deposited Mass

As noted, the incremental mass scavenged from a particle in a time step is recorded in a two-dimensional deposition array to which all particles may contribute. We wish to estimate the sensitivity of deposited mass to the rain rate (or particle size), i.e. the response of that deposit (cell-wise) to a perturbation in the input, from which we will later estimate the uncertainty in the deposition field. Overall we expect an increase in rain rate to promote more deposition. But the analysis of sensitivity for a deposition field within a transport calculation reveals a more complex story. Consider a single deposition from a specific particle *i*, occurring at time t_{n+1}. The incremental mass removed (and deposited) is:

$$\Delta m_i(t_{n+1}) = M_i(t_n) - M_i(t_{n+1}) \qquad \textbf{eq. 20}$$

The sensitivity of the deposited mass to the rain rate is then:

$$\frac{\partial(\Delta m_i)}{\partial \ln(J)} = \frac{\partial(M_i(t_n))}{\partial \ln(J)} - \frac{\partial(M_i(t_{n+1}))}{\partial \ln(J)} = S_i(t_n) - S_i(t_{n+1}) \qquad \textbf{eq. 21}$$

Or, using a Taylor's series notation, where the subscript *o* represents the nominal value (without consideration of uncertainties):

$$\begin{aligned} \delta m_i(t_{n+1}) &= M_{i,o}(t_n) + \Delta m(t_n) - M_{i,o}(t_{n+1}) - \Delta m(t_{n+1}) \\ &= M_{i,o}(t_n) + \left(\frac{\Delta J}{J}\right)\frac{\partial M_i}{\partial \ln(J)}(t_n) - M_{i,o}(t_{n+1}) - \left(\frac{\Delta J}{J}\right)\frac{\partial M_i}{\partial \ln(J)}(t_{n+1}) \qquad \textbf{eq. 22} \\ &= M_{i,o}(t_n) + \left(\frac{\Delta J}{J}\right)S_i(t_n) - M_{i,o}(t_{n+1}) - \left(\frac{\Delta J}{J}\right)S_i(t_{n+1}) \end{aligned}$$

The equation shows that the response of the deposited mass to the rain rate is described by the difference in sensitivity of the particle before and after deposition. As noted previously, particle sensitivities are typically negative in sign. In this case, a positively signed difference indicates that the sensitivity of the particle is increasing in magnitude, and an increase in rain rate would promote more deposition in the cell. Conversely, a negatively signed difference indicates that the sensitivity of the particle is decreasing in magnitude, and an increase in rain rate would promote less deposition in the cell. This would occur when an increase in rain rate caused earlier deposition of the particle mass, depleting mass and lessening downwind deposits. Hence the sign of the sensitivity of the deposited incremental mass conveys important information.

The "deposited" sensitivity is thus $S(t_n)$-$S(t_{n+1})$; i.e. it changes its sign when $S(t_n) = S(t_{n+1})$, at the root of equation 10:

$$t^* = \frac{1}{\lambda} \qquad \textbf{eq. 23}$$

The existence of differently signed sensitivities for the deposited mass raises the possibility of compensatory effects from different particles within a simulation. By way of example, consider a one-dimensional simulation, where a particle travels with a constant velocity through constant rain, depositing mass along the line it travels. Increasing the rain rate will cause the mass of the particle to be depleted earlier, generating more mass in deposition cells near the beginning of the particle transport (positive response to perturbation) and less mass in cells farther along (negative response). Alternately, a decrease in rain rate would generate less mass in the early cells and more in the cells farther along. Now imagine two such particles have deposited along the same path but encountered different rain rates: the first depositing 3 deposition units with a positive 0.1 response, the second depositing 2 units with a negative 0.5 response:

deposit 1:	3 units	+0.1 response
deposit 2:	2 units	- 0.5 response

To understand the total deposition in this cell, we must include the compensatory effects of the two. The total deposit is 5 units, with a response of –0.4; a higher rain rate would result in a lower deposition in the cell. The overall uncertainty on this deposit is 0.4 deposition units.

A suite of single-particle simulations is presented in the appendix, demonstrating the effects of different relative uncertainties on the deposited mass, for various particle sizes and rain rates.

Conclusion

First-order local sensitivity analysis provides a tool for exploring the sensitivity and uncertainty of model simulations to perturbations in input parameters. This work describes the use of such analysis to investigate and contrast the sensitivity of wet deposition processes to rain rate and particle size. Several important features have been identified. First, the magnitudes of the wet deposition sensitivity to particle size and rain rate are comparable, for the regimes of interest, indicating that both parameters must be known well for adequate simulation. The slightly greater sensitivity to particle size for certain particle sizes of interest suggests that source term characteristics can play a key role in overall uncertainty. Second, the derived deposition sensitivities change sign with distance downwind. As a result, deposition uncertainties show minima at some distance downwind (where the sensitivity, in changing sign, passes through zero). These results indicate that deposition sensitivities and uncertainties will evince complex patterns. Finally, the results of a sample simulation demonstrate that the air concentration uncertainties (with respect to wet deposition) can be small in a wet deposition environment.

This study explored only first-order local sensitivity analysis, and use of these sensitivities for uncertainty quantification relies on a truncated Taylor series. Hence, the acceptable perturbation size (or acceptable input uncertainty) is limited by the accuracy of that truncation. Nonetheless, this method provides a useful analysis for contrasting the sensitivities of the two parameters of interest and beginning to quantify the uncertainty associated with the phenomenon of interest.

Implementation into a Lagrangian dispersion code was straightforward for wet deposition processes, in which the quantity of interest (particle mass) followed a straightforward relationship with the input parameters. This methodology is likely not appropriate for an overall uncertainty quantification of plume transport, in which the meteorological input uncertainties (wind speed and direction) are poorly quantified and influence particle transport in numerous complex ways (such as through turbulent parameterizations).

Acknowledgements

This work has benefited greatly from the expertise and ongoing research in sensitivity analysis at the Center for Applied Scientific Computing (CASC). This work was performed under the auspices of the U. S. Department of Energy by the University of California, Lawrence Livermore National Laboratory under Contract No. W-7405-Eng-48.

Appendix: Test Cases

A suite of simulations was executed with constant λ to explore the results of the sensitivity and uncertainty calculations. The constant values of λ were obtained by fixing the particle size and rain rate, and the values chosen were meant to demonstrate different features. For simplicity, all simulations were executed with one particle only, and for each of the simulations, the particle mass trace and deposited mass were computed, along with the sensitivities of each to particle size and rain rate. Dry deposition was not computed, so all depositions described below include wet deposition only. Different values of uncertainties in rain rate and particle size were used to compute uncertainties on the mass remaining in the particle and the deposited mass. A subset of the simulations are presented here, as summarized in Table 1:

Table 1: Simulations for sensitivity testing

figure	case number	particle size [m]	rain rate [mm/hr]	lambda [1/s]	comments
12	3	5e-6	1	9.27e-5	Chosen to show range of lambdas. $\lvert S_{dp}\rvert > \lvert S_J\rvert$. (see Figure 7).
13	5	5e-6	50	2.04e-3	
14	7	5e-6	150	4.62e-3	
15	8	5e-7	150	2.99e-6	$\lvert S_J\rvert > \lvert S_{dp}\rvert$, $S_{dp} > 0$. (Increasing particle size => smaller λ and less mass removed).
16	9	1.5e-5	5	1.41e-3	$\lvert S_J\rvert > \lvert S_{dp}\rvert$, $S_{dp} < 0$.

Table 2: List of figures (key to Figures 12-16) for simulation results

cases:	contain:
particle mass over time (a)	• particle mass over time • particle mass uncertainty given $\sigma_J = \sigma_{dp} = 1\%$ • upper and lower bound (mass ± uncertainty) • relative uncertainty = (uncertainty ÷ remaining mass)
particle mass over time (b)	• particle mass sensitivities to rain rate and particle size • particle mass uncertainties for: $\sigma_J = \sigma_{dp} = 1\%$ $\sigma_J = 10\%$ & $\sigma_{dp} = 1\%$ $\sigma_J = 1\%$ & $\sigma_{dp} = 5\%$
deposited mass by cell (c)	• deposited mass by grid cell at simulation end • deposited mass uncertainty given $\sigma_J = \sigma_{dp} = 1\%$ • upper and lower bound (mass ± uncertainty) • relative uncertainty = (uncertainty ÷ deposited mass)
deposited mass by cell (d)	• deposited mass sensitivities to rain rate and particle size • deposited mass uncertainties for: $\sigma_J = \sigma_{dp} = 1\%$ $\sigma_J = 10\%$ & $\sigma_{dp} = 1\%$ $\sigma_J = 1\%$ & $\sigma_{dp} = 5\%$

Figure 12 (case 3a)

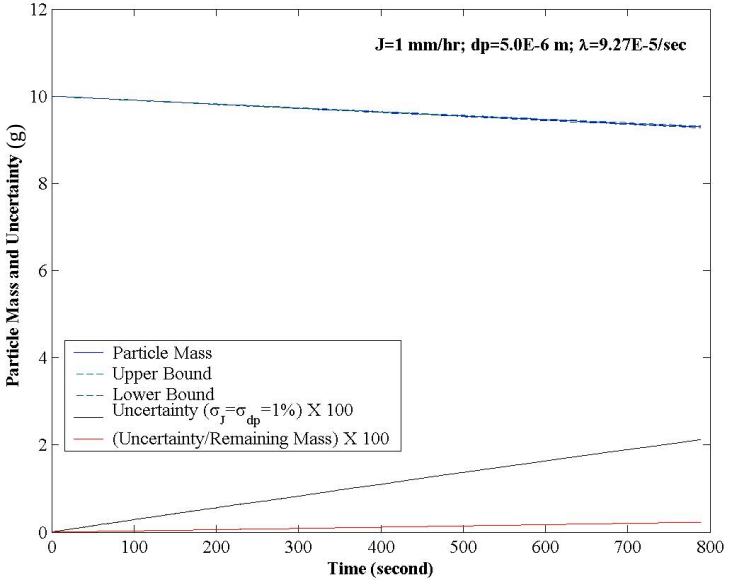

(case 3b)

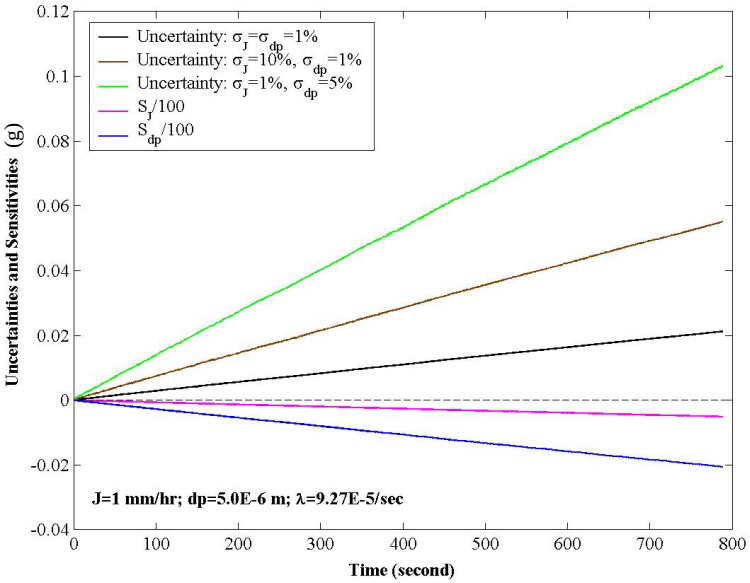

(case 3c)

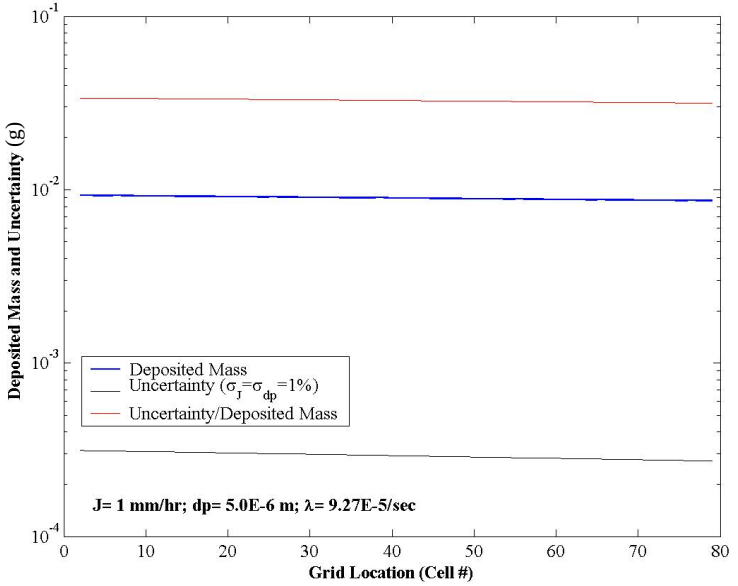

(case 3d)

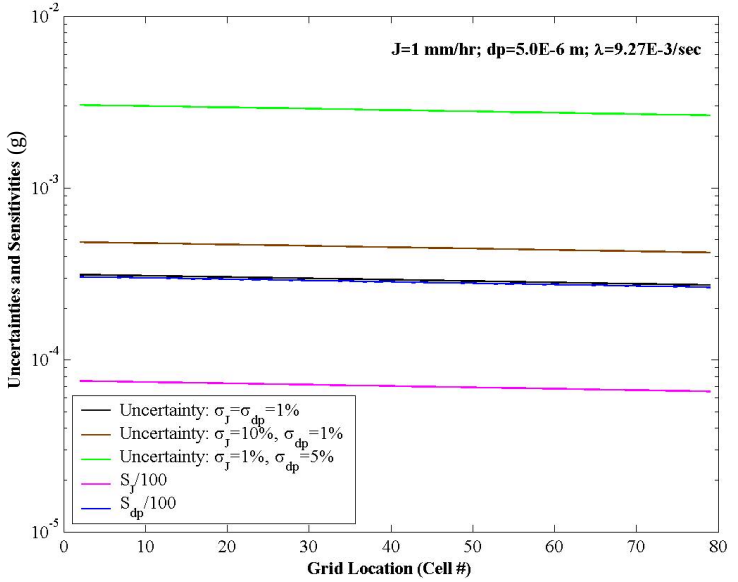

Figure 13 (case 5a)

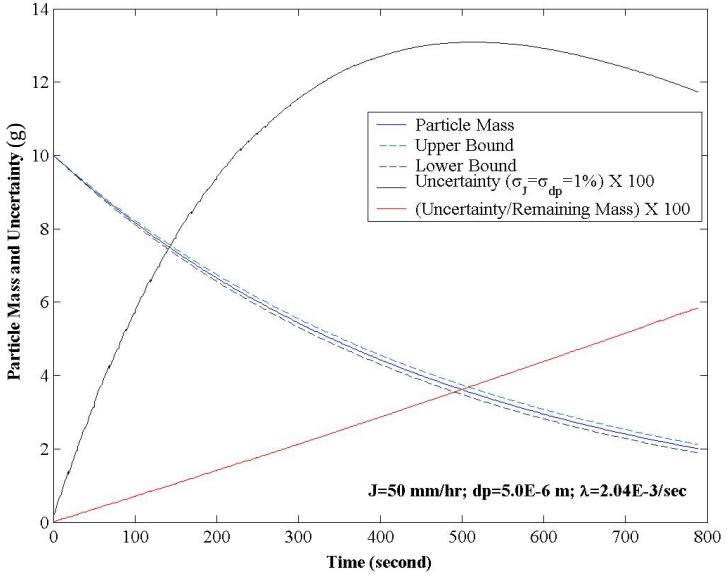

(case 5b)

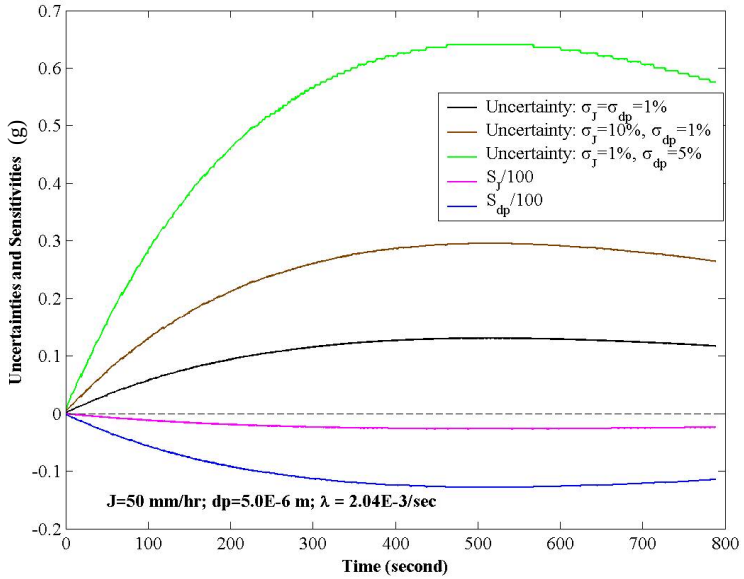

(case 5c)

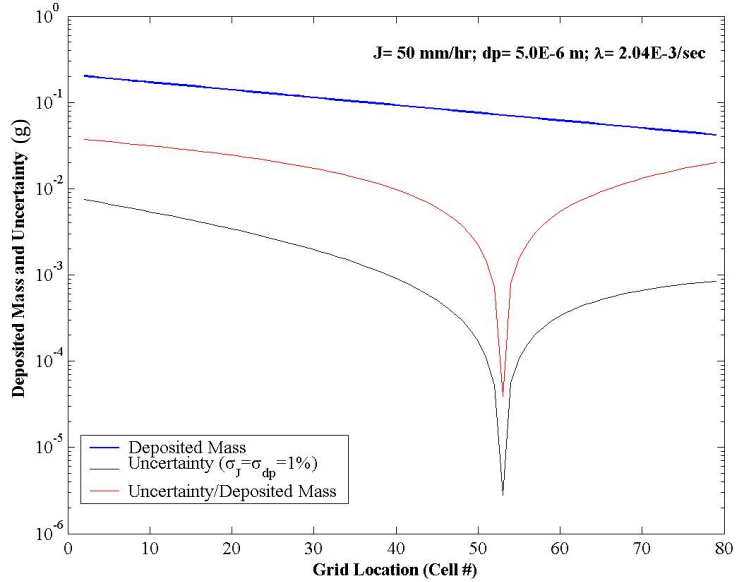

(case 5d)

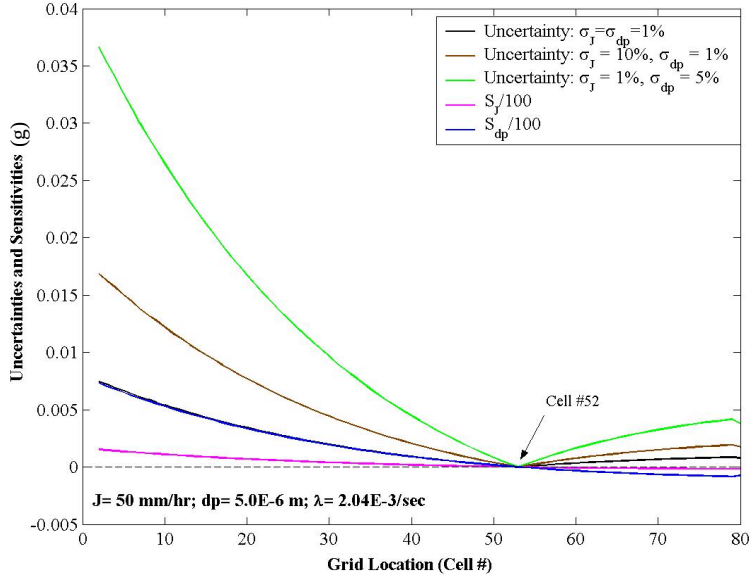

Figure 14 (case 7a)

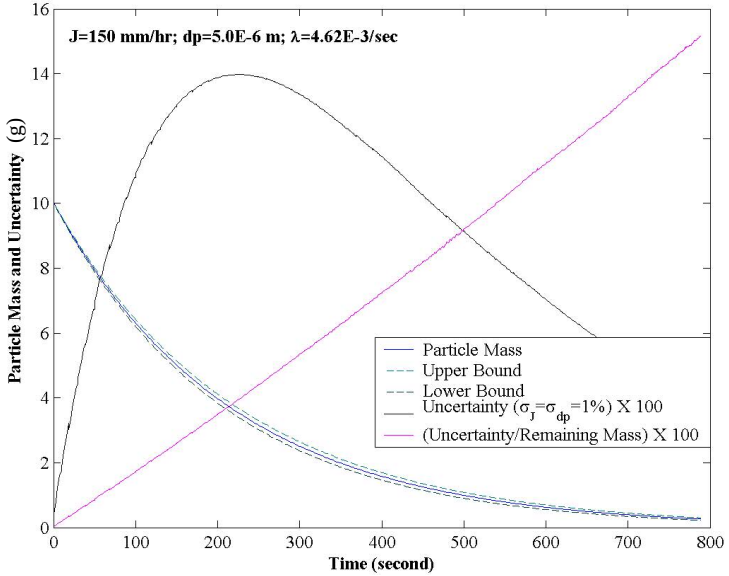

(case 7b)

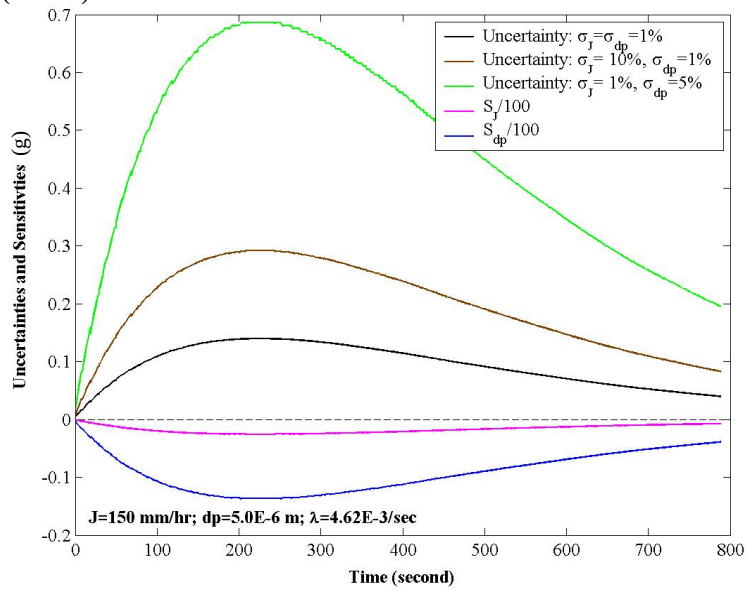

(case 7c)

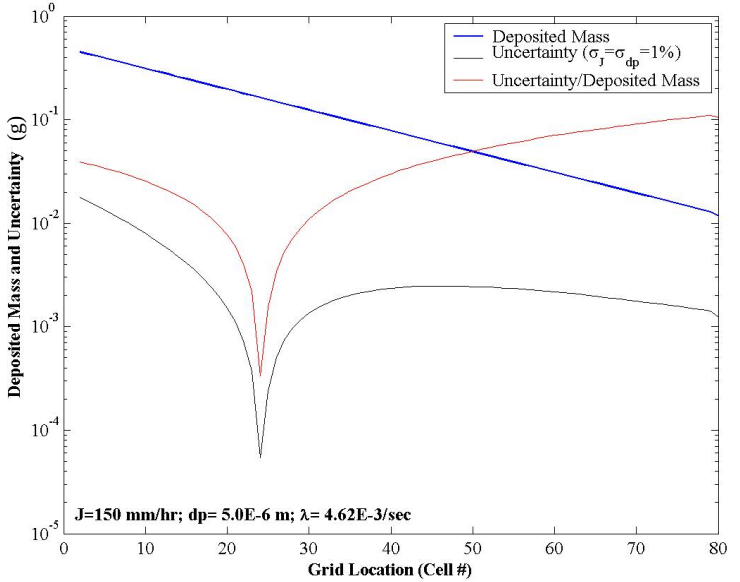

(case 7d)

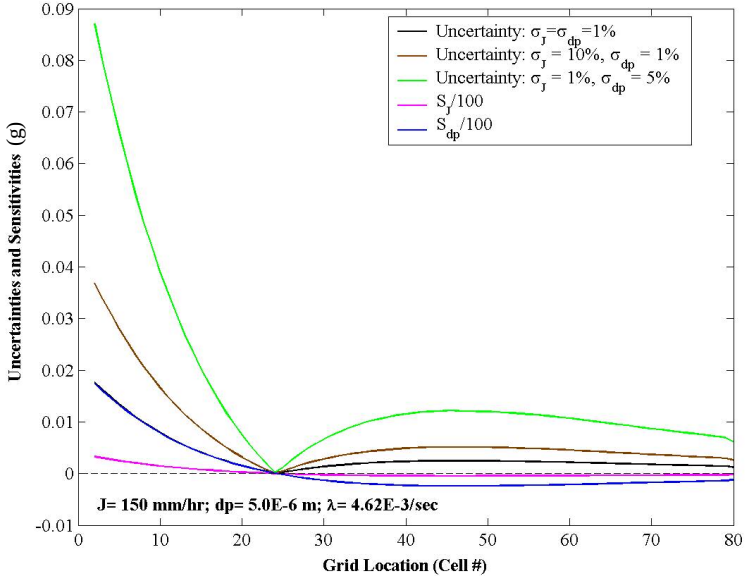

Figure 15 (case 8a)

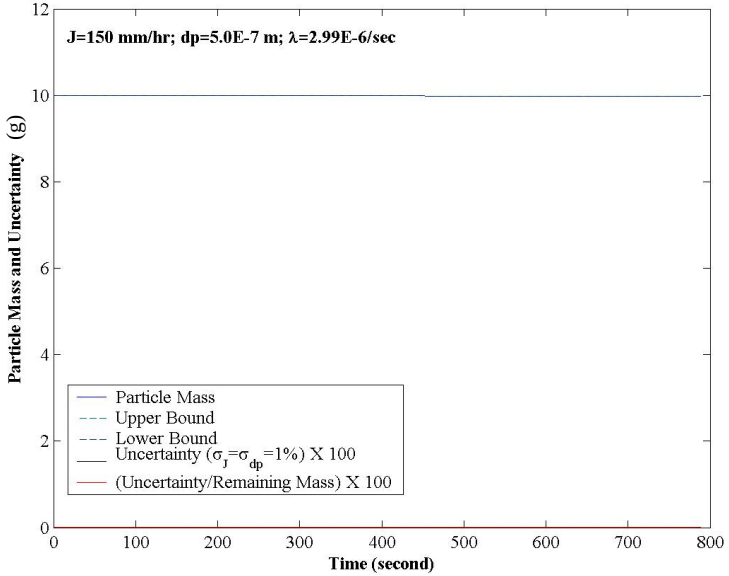

(case 8b)

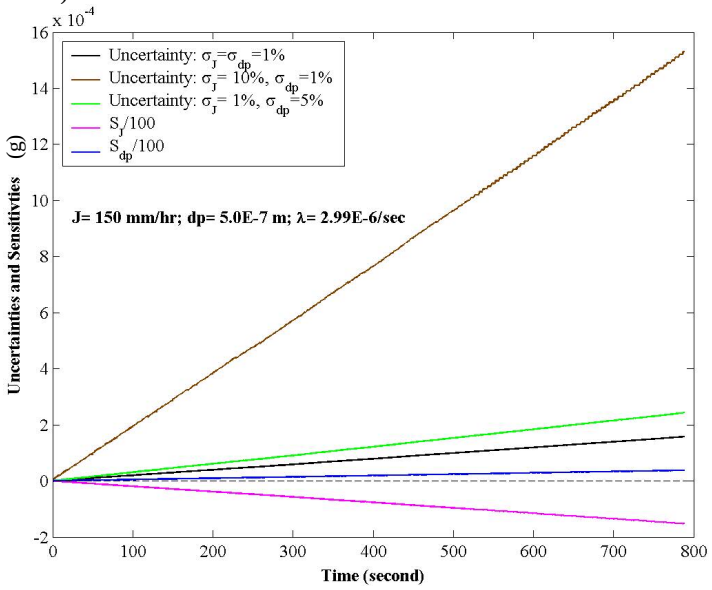

(case 8c)

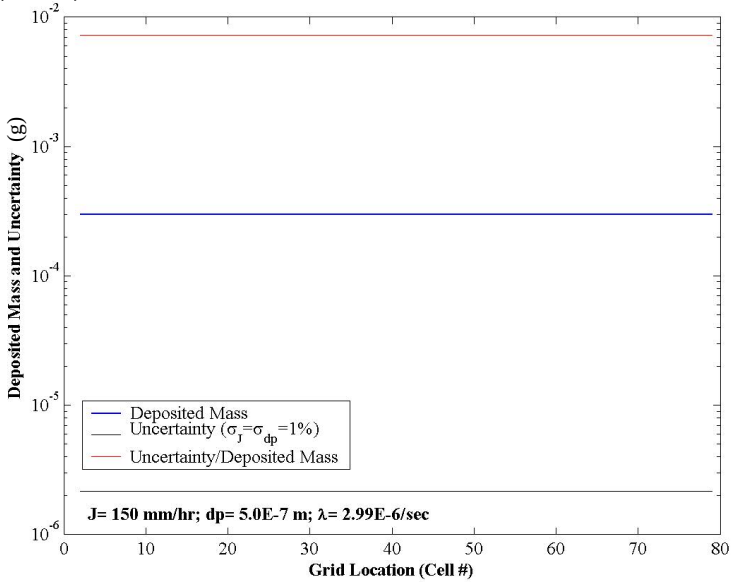

(case 8d)

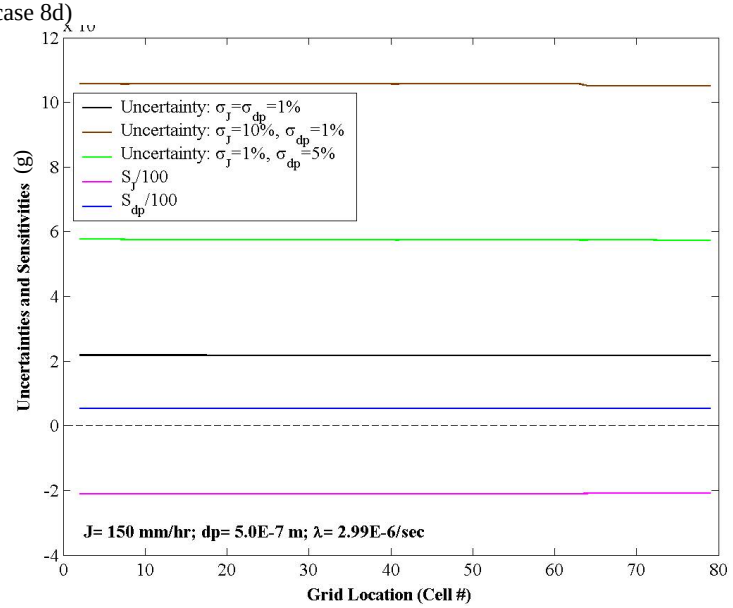

Figure 16 (case 9a)

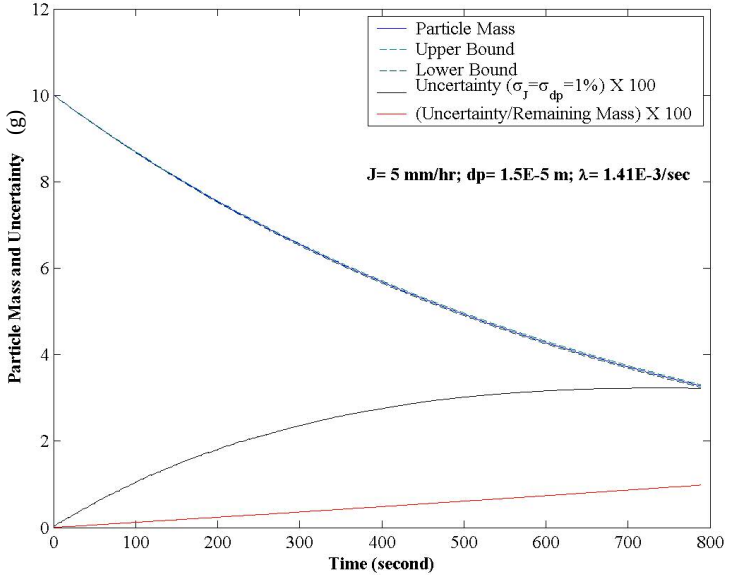

(case 9b)

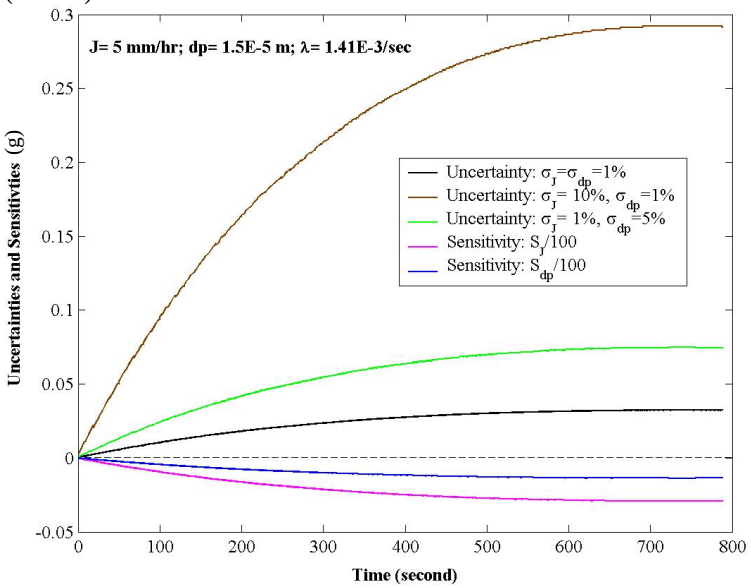

(case 9c)

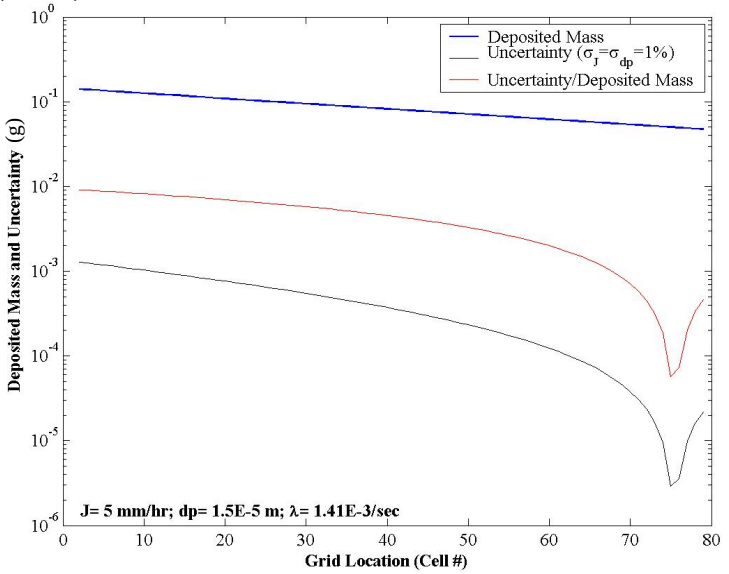

(case 9d)

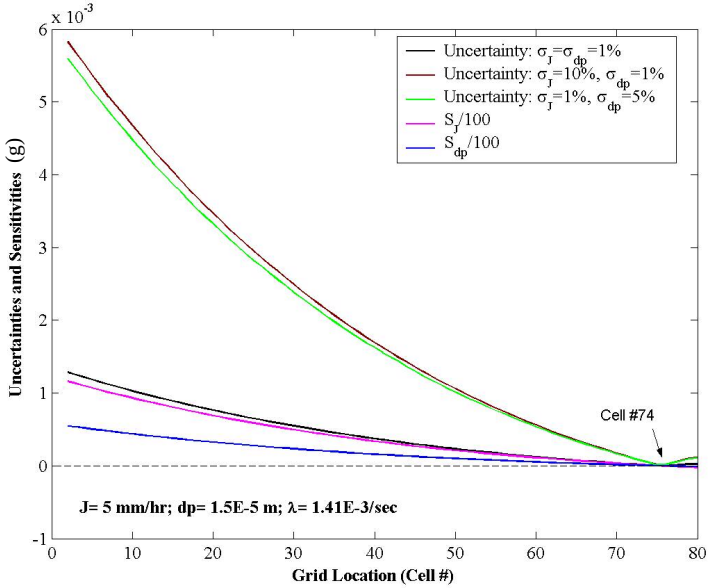

Figures 17 and 18 explore the effect of particle size and rain rate on the particle mass.

Figure 17: Particle mass decaying over time, for two different particle sizes

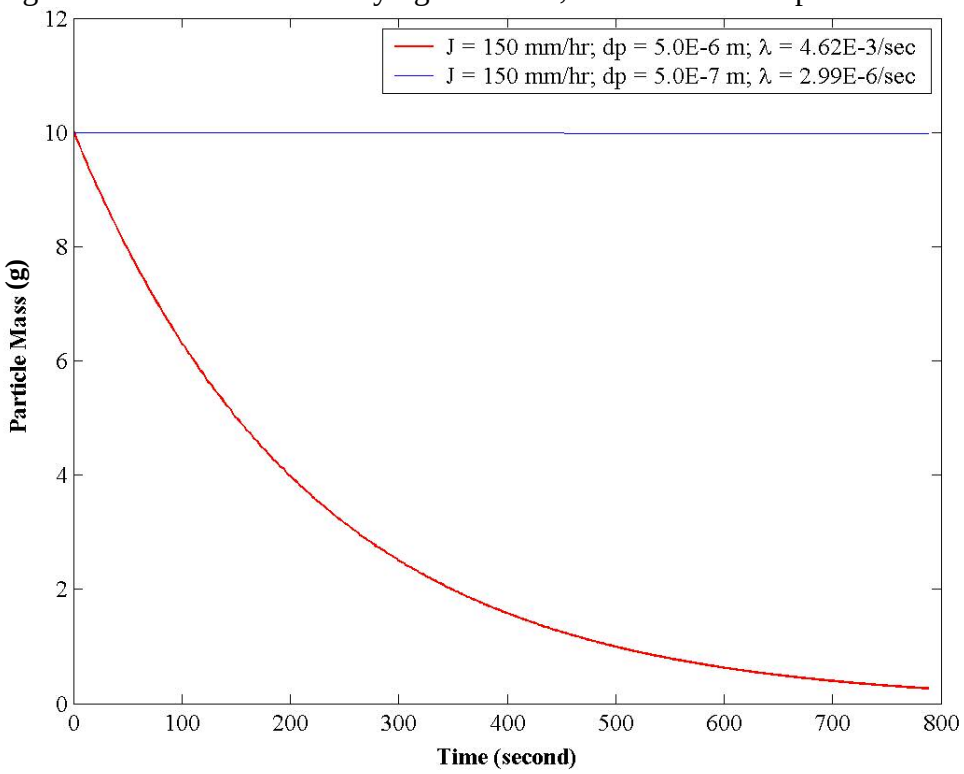

Figure 18: Particle mass decaying over time for different rain rates.

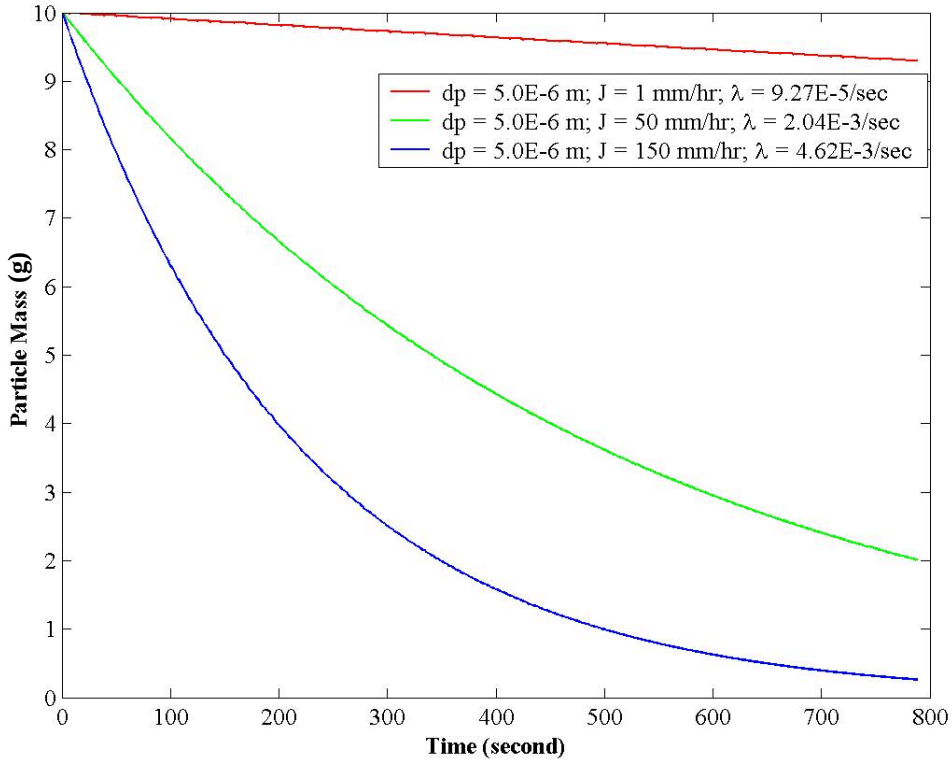

Figures 19 and 20 show the effect of rain rate on the deposited mass.

Figure 19: Deposited mass as a function of rain rate.

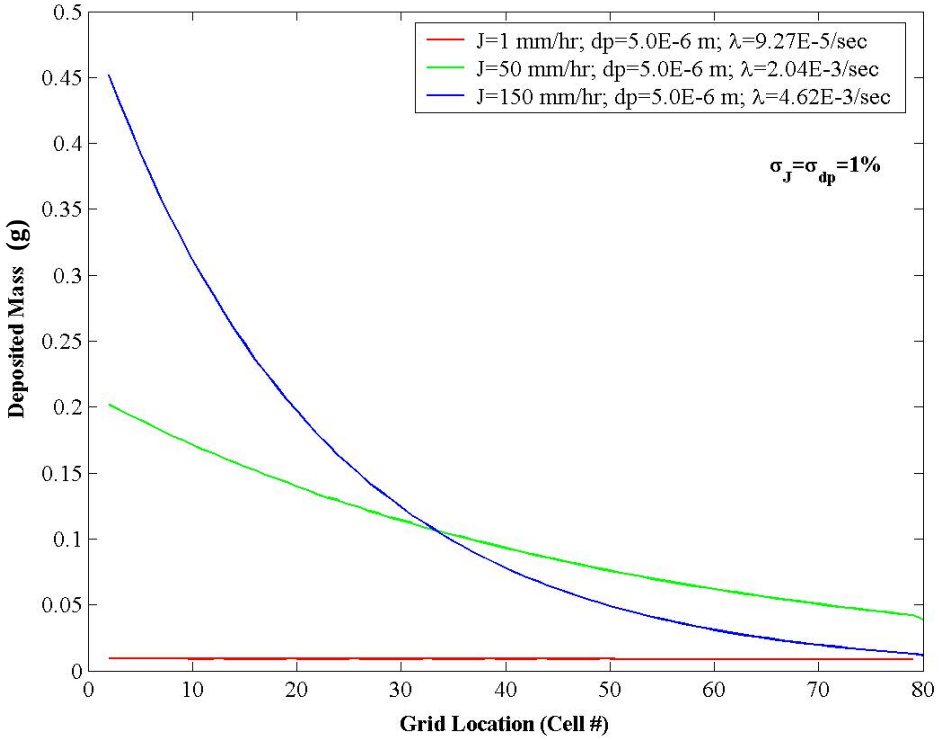

Figure 20: Uncertainty in deposited mass as a function of rain rate

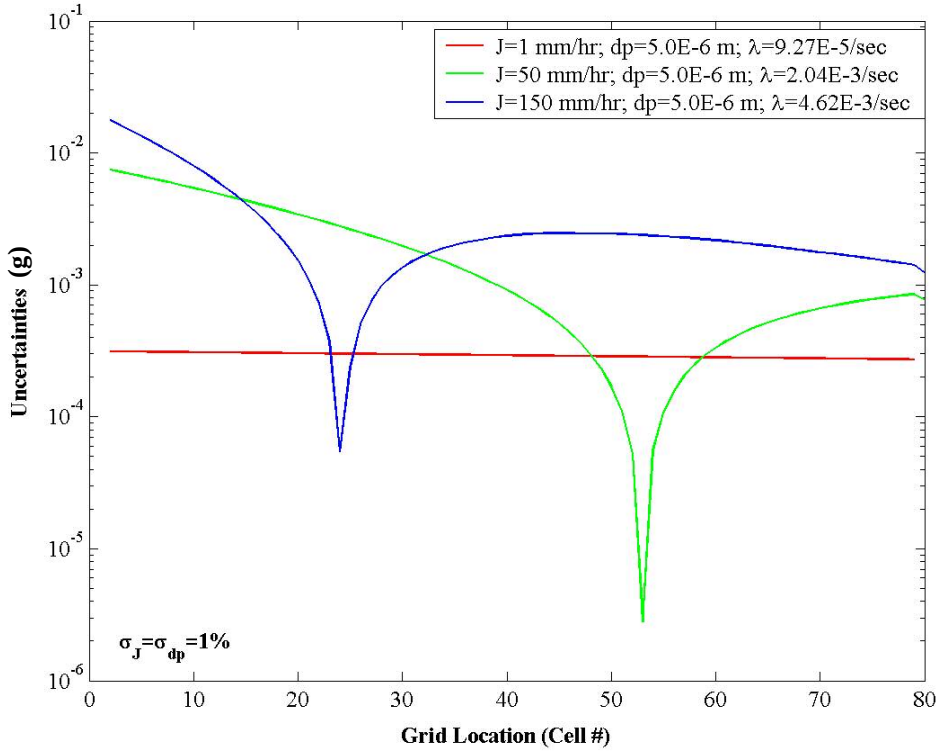

Figures 21 and 22 show the effect of particle size on the deposited mass.

Figure 21: Deposited mass as a function of particle size

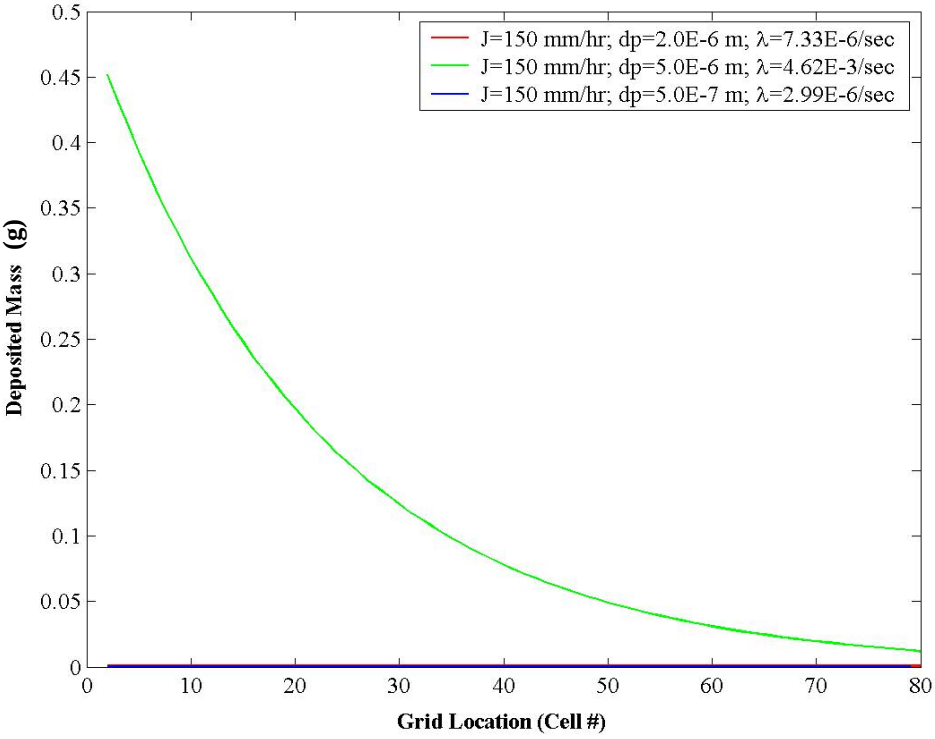

Figure 22: Uncertainty in deposited mass as a function of rain rate.

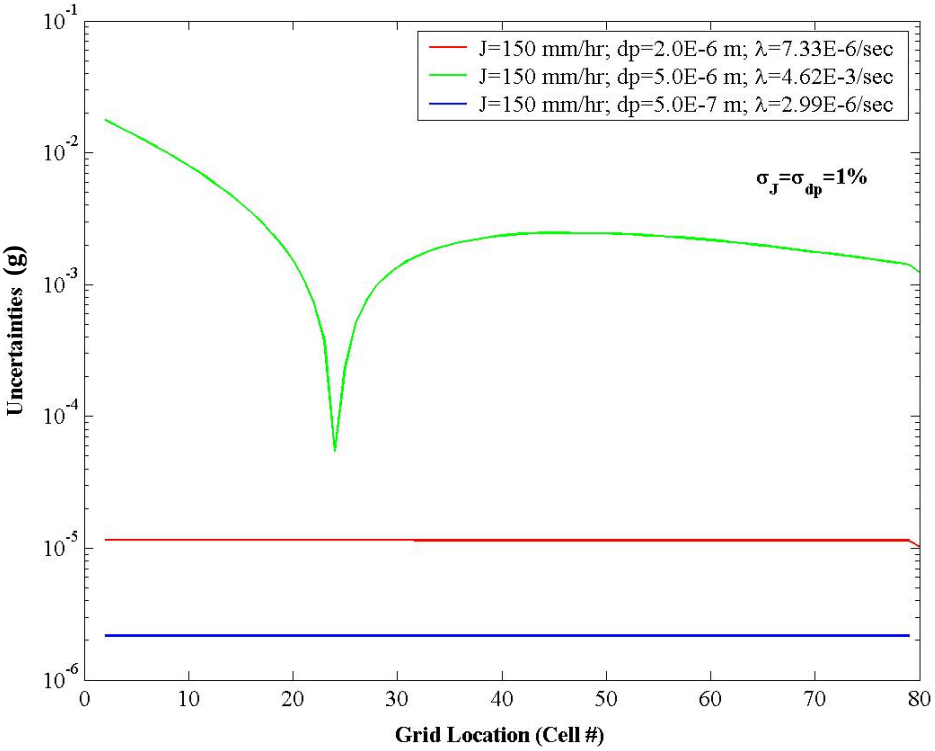

Figures 23 and 24 show the time evolution of sensitivity to particle size and rain rate.

Figure 23: Magnitude of sensitivity to rain rate over time

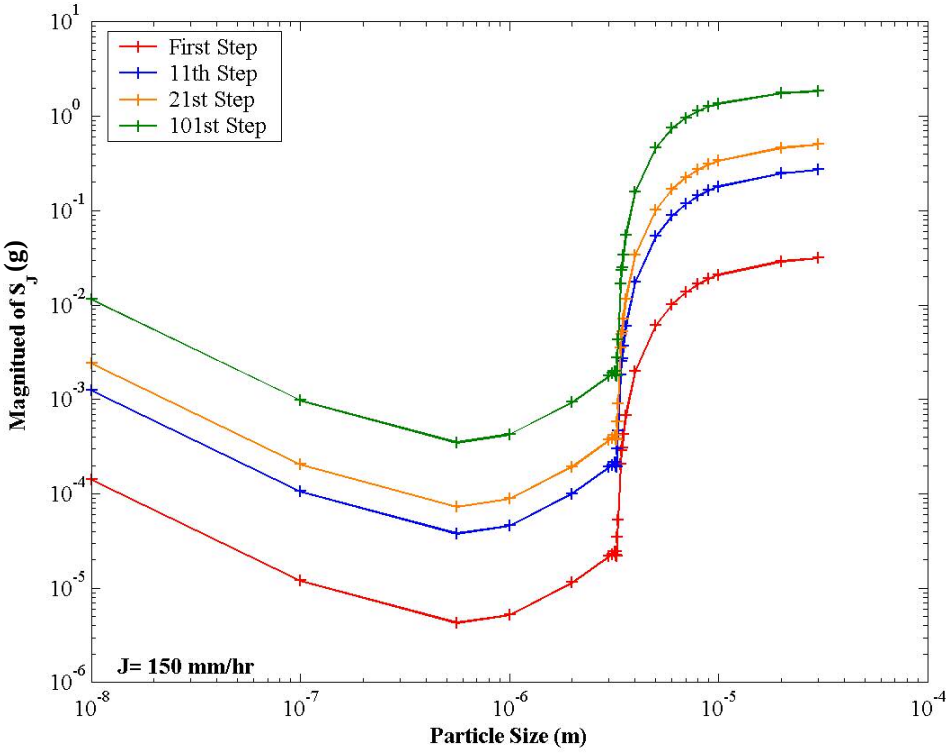

Figure 24: Magnitude of sensitivity to particle size over time

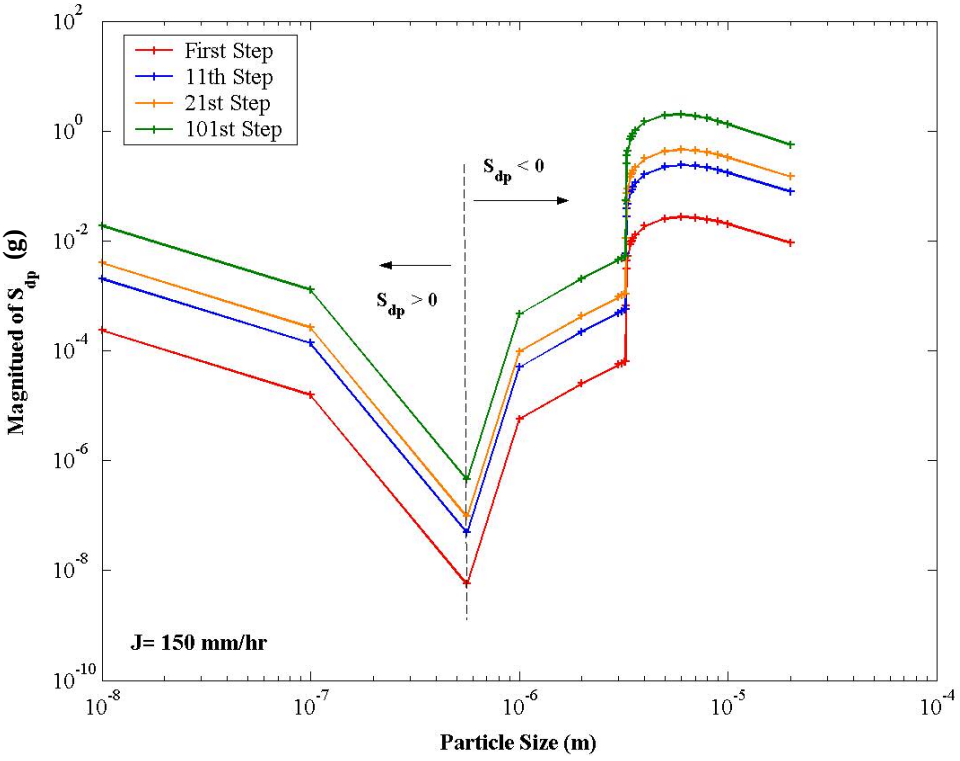

References

1. Ermak, D.L. and J.S. Nasstrom, *A Lagrangian stochastic diffusion method for inhomogeneous turbulence.* Atmospheric Environment, 2000. **34**(7): p. 1059-1068.
2. Sugiyama, G. and S.T. Chan. *A New Meteorological Data Assimilation Model for Real-Time Emergency Response*. in *10th Joint Conference on the Applications of Air Pollution Meteorology*. 1998. Phoenix, AZ: American Meteorological Society.
3. Hodur, R.M., *The Naval Research Laboratory's Coupled Ocean/Atmosphere Mesoscale Prediction System (COAMPS).* Mon. Wea. Rev., 1997. **125**: p. 1414-1430.
4. Loosmore, G.A. and R.T. Cederwall, *Precipitation Scavenging for Emergency Response Applications: Testing an Updated Model with New Real Time Data*. 2003, LLNL: Livermore.